Development of Channeled Nanofibrous Scaffolds for Oriented Tissue Engineering

Chenghui Sun, Xiaobing Jin, Jeremy M. Holzwarth, Xiaohua Liu, Jiang Hu, Melanie J. Gupte, Yaoming Zhao, Peter X. Ma*

A tissue-engineering scaffold resembling the structure of the natural extracellular matrix can often facilitate tissue regeneration. Nerve and tendon are oriented micro-scale tissue bundles. In this study, a method combining injection molding and thermally induced phase separation techniques is developed to create single- and multiple-channeled nanofibrous poly(L-lactic acid) scaffolds. The overall shape, the number and spatial arrangement of channels, the channel wall matrix architecture, the porosity and mechanical properties of the scaffolds are all tunable. The porous NF channel wall matrix provides an excellent microenvironment for protein adsorption and the attachment of PC12 neuronal cells and tendon fibroblast cells, showing potential for neural and tendon tissue regeneration.

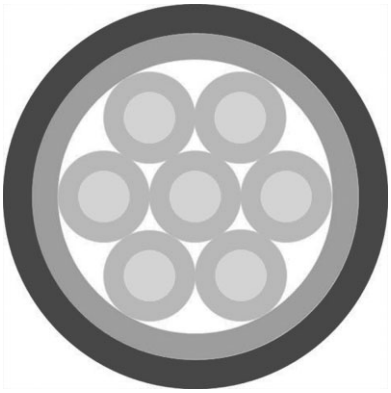

1. Introduction

Tissue engineering aims to develop biologically functional living substitutes for traumatized and diseased tissues.[1] It is often beneficial for a tissue-engineering scaffold to resemble the structure and properties of the native tissue in terms of facilitating cell differentiation and tissue regeneration.[2–4] For example, hydrogels, having similar structural features and mechanical properties to those of cartilage extracellular matrix (ECM), have been shown to facilitate chondrocyte differentiation and to enhance the chondrocyte phenotype.[5,6] Nanofibers, having similar architecture to that of collagens in bone and cartilage matrix, have been demonstrated to facilitate both bone and cartilage regeneration.[7–10] More and more tissue engineers take the biomimetic approach to design three-dimensional (3D) scaffolds, mimicking the architecture and properties of the ECM, to facilitate the desired tissue regeneration.[2,11] The nerve ECM is composed predominantly of collagen fibers, forming an oriented multi-leveled tubular bundle structure.[12] The tendon ECM is characterized by aligned bundle structures consisting of collagen nanofibers.[13] Since anisotropic physical cues in a scaffold may advantageously facilitate neuronal axon formation and tendon tissue alignment,[14–16] considerable efforts have been devoted to creating channeled scaffolds to engineer these bundled tissues. For example, multiple-channeled scaffolds have been fabricated using molding[14,17,18] and templating techniques.[19,20] However, these scaffolds failed to emulate the nanofibrous (NF) morphology of collagen fibers, which were found to be important in regulating cell behavior and tissue function.[7,21] While 3D NF scaffolds have been developed using an electrospinning technique,[22] it remains challenging to

C. Sun, Dr. X. Jin, Dr. X. Liu, Dr. J. Hu, Prof. P. X. Ma
Department of Biologic and Materials Sciences, University of Michigan, Ann Arbor, MI 48109, USA
E-mail: mapx@umich.edu
C. Sun, Prof. Y. Zhao
College of Materials Science and Engineering, South China University of Technology, Guangzhou 510640, China
J. M. Holzwarth, M. J. Gupte, Prof. P. X. Ma
Department of Biomedical Engineering, University of Michigan, Ann Arbor, MI 48109, USA
Prof. P. X. Ma
Macromolecular Science and Engineering Center, Department of Materials Science and Engineering, University of Michigan, Ann Arbor, MI 48109, USA

DOI: 10.1002/mabi.201200004

electrospin biomaterials into a 3D scaffold with an anatomical shape or a designed pore network.[23] NF matrix can also be fabricated using self-assembly techniques,[24] but the self-assembled hydrogels lack sufficient mechanical strength to stabilize the intricate channel structure,[2] limiting their applications. A thermally induced phase separation (TIPS) technique has been developed in our lab to generate NF scaffolds from various biodegradable polymers.[25,26] By combining the new TIPS technique with a molding technique, we developed single- and multiple-channeled NF poly(L-lactic acid) (PLLA) scaffolds in this work. The morphology and mechanical properties of the scaffolds were characterized, and their interactions with neuronal cells and tendon fibroblast (FB) cells were examined.

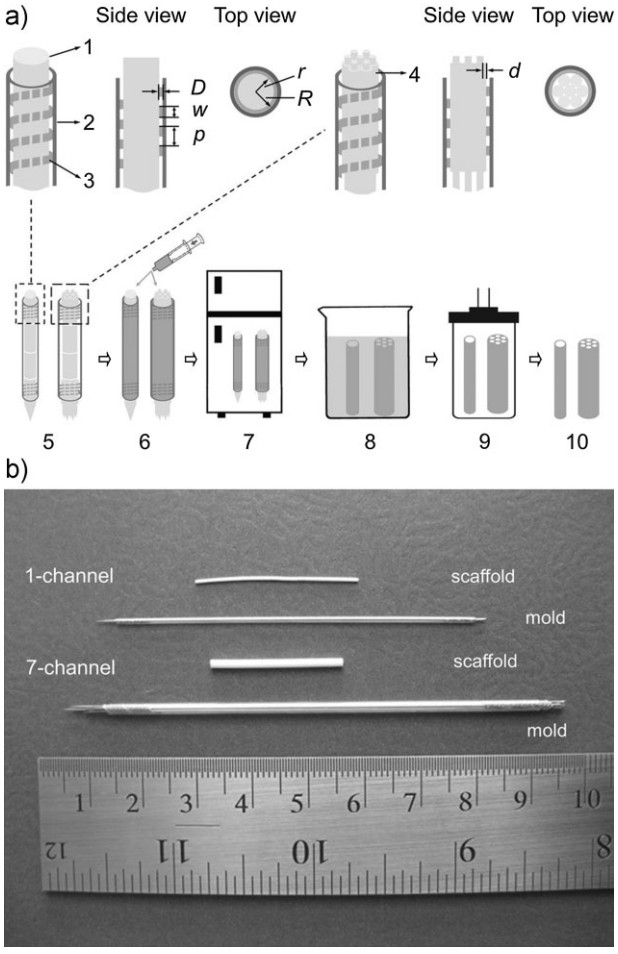

Figure 1. (a) Schematic illustration of the mold design and the fabrication of NF scaffolds with longitudinally aligned channels. The molds were composed of a varying number of acupuncture needles (1) inserted into a glass capillary tube (2) with helical tapes alone (3) or together with a bundle of short sleeves on both ends of the needles (4). The inner radius of the glass capillary tube is *R*; the radius of the acupuncture needle is *r*; the helical tape thickness is *D*, the pitch is *p*, the width is *w*, and the sleeve thickness is *d*. Single and multiple channeled scaffolds (10) were produced by a series of steps: mold assembly (5), PLLA/THF solution injection (6), phase separation (7), mold removal, solvent exchange (8), and freeze drying (9). (b) Appearance of the molds and as-prepared NF PLLA scaffolds with either a single channel or seven channels.

2. Experimental Section

2.1. Materials

PLLA with an inherent viscosity of 1.6 $dL \cdot g^{-1}$ was purchased from Boehringer Ingelheim (Ingelheim, Germany). Tetrahydrofuran (THF) and dichloromethane (DCM) were purchased from Fisher Scientific (Pittsburgh, PA, USA).

2.2. Preparation of Scaffolds

The molds were assembled by inserting a varying number of acupuncture needles into a glass capillary tube with pre-located spacers at both ends, as schematically illustrated in Figure 1a. A single needle and a pair of helical tapes were used to fabricate a single-channeled scaffold, while four or seven needles with short sleeves at both ends were used to create multiple-channeled scaffolds. PLLA solutions in THF of varying concentrations from 6 to 12% w/v were injected into the molds, followed by phase separation at −80 °C for 12 h. The molds containing the gelled polymer solutions were then transferred into ice-cold distilled water to release the needles from the scaffold and to exchange the solvent with water. Distilled water was changed six times over a course of 48 h and the samples were removed from the glass tube during the first 6 h of solvent exchange. After that, samples were frozen at −80 °C for 4 h and lyophilized for 48 h to obtain the channeled NF scaffolds. The same molds were used to fabricate solid-walled (SW) control scaffolds using a solvent evaporation method. PLLA solution in DCM was injected into the molds and placed in a fume hood to allow the solvent to evaporate at room temperature for 24 h. Then, the scaffolds were demolded and placed in a vacuum desiccator to further remove the solvent. All the dried scaffolds were trimmed and kept in a desiccator until use.

The NF PLLA films with a thickness around 40 μm were fabricated using casting and phase separation techniques as previously described.[27] The solid PLLA films were generated in a similar manner but without the phase separation process. Instead, the solvent was removed by evaporation at room temperature in a fume hood for 24 h. All the films were cut into the shape and size to fit in the wells of a 12-well tissue culture plate and kept in a desiccator until use.

2.3. Characterization of Scaffolds

The morphology of the scaffolds was examined using scanning electron microscopy (SEM, Philips XL30 FEG). To expose the internal and cross-sectional architecture, a sample was fractured after being frozen in liquid nitrogen for several minutes. The sample was coated with gold using a sputter coater (Desk-II, Denton vacuum

Inc.), and was analyzed at 10 kV. The average fiber diameter and fiber length of the exposed surface were subsequently calculated from the SEM micrographs using ImageJ software (National Institutes of Health). At least 100 fibers were measured for each sample, and the average and standard deviation (SD) were reported. The surface area was measured using nitrogen adsorption experiments at liquid nitrogen temperature on a Belsorp-Mini surface area analyzer (Bel Japan, Osaka, Japan) after evacuating samples at 25 °C for 10 h ($<7 \times 10^{-3}$ Torr). The density of the PLLA scaffold (D_f) was calculated from the volume and the mass. The volume was calculated from the inner-diameter, outer-diameter, and length of each scaffold. The mass of each scaffold was measured with an analytical balance.

The porosity was defined as $\varepsilon = 1 - D_f/D_p$, where the skeletal density (D_p) was given by

$$D_p = \frac{1}{(1 - X_c/D_a) + (X_c/D_a)}$$

where the degree of crystallinity (X_c) was measured by DSC as described previously.[25] The density of amorphous PLLA (D_a) is 1.248 $g \cdot cm^{-3}$, and the density of 100% crystalline PLLA (D_c) is 1.290 $g \cdot cm^{-3}$.

The tensile mechanical properties of single channeled NF PLLA scaffolds (2 mm inner diameter, 160 μm wall thickness) prepared from various polymer concentrations were tested uniaxially using an MTS Synergie 200 mechanical tester (MTS Systems Corporation, Eden Prairie, MN, USA). A gauge length of 10 mm and a crosshead speed of 5 $mm \cdot s^{-1}$ were used. At least six specimens were tested for each sample. Data were collected from the specimens that failed in the middle.

2.4. Protein Adsorption

Both NF and SW scaffolds were soaked in 70% ethanol for 30 min, washed three times with phosphate-buffered saline (PBS, Gibco BRL, Grand Island, NY, USA) for 30 min each, and then soaked in 1% bovine serum albumin (BSA, Sigma, Saint Louis, MO, USA) for 2 h. Then, the scaffolds were washed in PBS and the protein adsorbed onto the scaffolds was collected in 1% sodium dodecyl sulfate (Aldrich Chemical Company, Milwaukee, WI, USA) as previously described.[28] The amount of protein was quantified using a Micro BCA Protein Assay Kit (Pierce, Rockford, IL, USA). The distribution of adsorbed protein on the scaffolds was observed using a confocal laser-scanning microscope (Nikon Eclipse C1, Japan). Briefly, the fluorescein isothiocyanate-conjugated BSA (FITC-BSA, 67 kDa, Sigma) was first adsorbed on the NF and SW scaffolds, and then the fluorescence images of the scaffolds were captured at the setting where fluorescent signals could not be seen from the control blank scaffolds.

2.5. Cell Culture

Rat adrenal pheochromocytoma cell line PC12 Adh cells (PC12 cells) were purchased from the American Type Culture Collection (ATCC Number: CRL-1721.1) and cultured according to the ATCC's protocol. The cells were cultured in ATCC-formulated F-12K Medium supplemented with 15% heat-inactivated horse serum (Invitrogen, Carlsbad, CA, USA), 2.5% fetal bovine serum (FBS, Gibco BRL), 100 $U \cdot mL^{-1}$ penicillin (Gibco BRL), and 100 $\mu g \cdot mL^{-1}$ streptomycin (Gibco BRL). The primary tendon FBs were isolated from 3–4 week-old New Zealand white rabbits (Harlan Sprague Dawley, MI, USA). The animal procedures were performed according to the protocol approved by the University of Michigan Committee of Use and Care of Laboratory Animals. The patellar tendon was removed from the hind legs and cut into small pieces, followed by digestion in 0.2% type I collagenase overnight under continuous shaking. The isolated primary patellar tendon FBs were then cultured in high glucose Dulbecco's modified Eagle's medium (Gibco BRL) supplemented with 10% FBS, 100 $U \cdot mL^{-1}$ penicillin, and 100 $\mu g \cdot mL^{-1}$ streptomycin.

2.6. Cell Seeding and Adhesion on Films

Both sterile NF and solid films were first soaked in 70% ethanol for 30 min and washed in PBS for three times for 30 min each and assembled on the bottoms of the 12-well cell culture plates. They were then immersed in complete media twice for 1 h each. PC12 cells and patellar tendon FBs were detached from the Petri dishes by the treatment of 0.25% trypsin/EDTA solution (Gibco BRL). 2×10^5 cells were seeded on each film and cultured in a humidified incubator at 37 °C with 5% CO_2 for 2 h. Then the unattached or loosely adherent cells were gently washing off and the collected cells (N) were counted using a hemocytometer. The proportion of cell attachment (P) was defined as: $P = 1 - N/(2 \times 10^5)$. Three NF and three SW films were used for each type of cells.

2.7. Cell Distribution in the Channeled Scaffolds

Single-channeled NF and SW scaffolds with an inner diameter of 700 μm and a length of 5 mm were used for cell culture. The sterile scaffolds were pre-treated similarly to the films and seeded with 4×10^5 cells. The cell-scaffold constructs were then cultured for 4 d. The samples were rinsed in PBS, fixed with 2.5 vol% glutaraldehyde in PBS at 4 °C for 24 h. After being thoroughly washed with PBS, the samples were treated with 1% osmium tetraoxide in 0.1 M cacodylate buffer for 1 h. The samples were then dehydrated in graded ethanol and then dried with hexamethyldisilazane (HMDS). The samples were sliced to expose the inner side and sputter-coated with gold before SEM observation.

2.8. Statistical Analysis

All data were presented as mean ± SD. To test the significance of observed differences between the study groups, an unpaired Student's t-test was applied. A value of $p < 0.05$ was considered to be statistically significant.

3. Results

In this study, injection molding was combined with a TIPS technique to create open channeled NF scaffolds. First, a mold was assembled by inserting a varying number of long

needles into a glass capillary tube with specially designed spacers, such as a pair of helical tapes alone or together with multiple short sleeves (tubular spacers on the ends of individual needles), which created the gaps for polymer solution to flow in and to form the channel walls of the scaffolds (Figure 1a). Channeled NF PLLA scaffolds were generated following a series of processing steps: PLLA/THF solution injection, TIPS, demolding, and solvent removal. The representative molds and scaffolds are shown in Figure 1b. The generated scaffolds replicated the reversed structures of the molds. SEM images revealed that the geometry of the channels was consistent through the entire length of the scaffolds (Figure 2). The channel diameter and wall thickness of the scaffolds were controlled by the needle size and the spacer thickness and could be easily altered. As an example, single channeled scaffolds with different inner diameters were created. The smaller single-channeled scaffold had an inner diameter of 400 μm and a wall

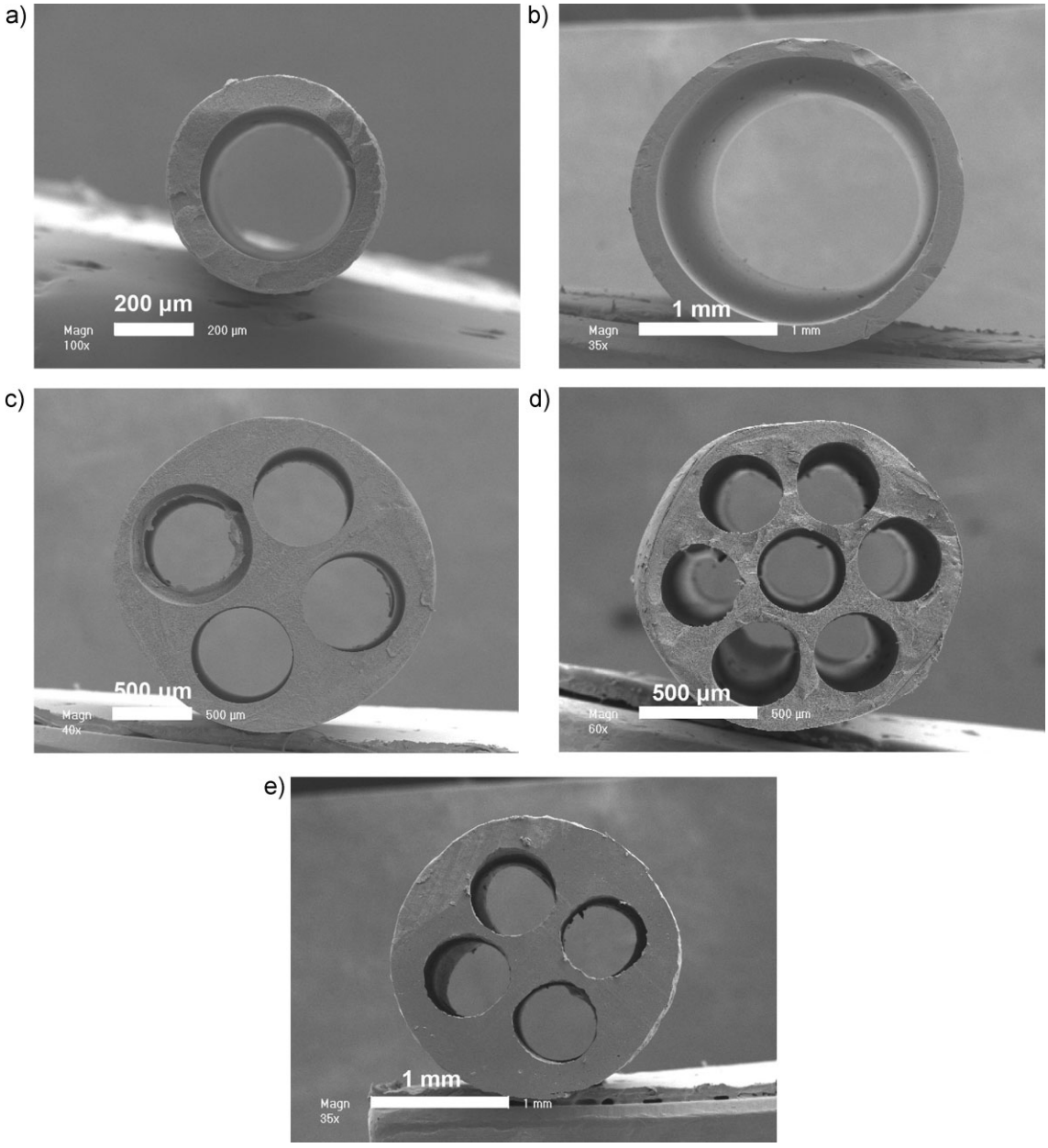

Figure 2. SEM micrographs of single and multiple channeled NF PLLA scaffolds with varying geometric parameters (a–d) and an SW PLLA scaffold (e) at low magnifications. All NF scaffolds were prepared by phase separation of 8% w/v PLLA/THF solution at −80 °C. The SW scaffold (e) was generated by solvent evaporation from a 20% w/v PLLA/DCM solution at room temperature, after injection into the same mold as that used for (c).

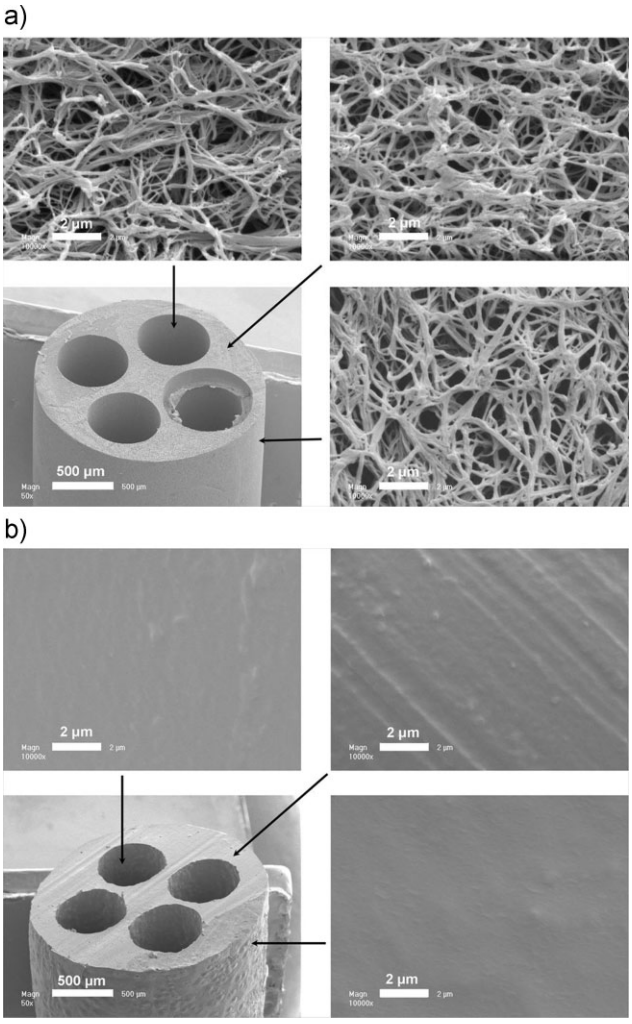

Figure 3. High magnification SEM micrographs showing wall morphology of channeled scaffolds: (a) 4-channel NF PLLA scaffold, (b) 4-channel SW PLLA scaffold.

thickness of 60 μm (Figure 2a) while the larger single-channeled scaffold had an inner diameter of 2 mm and a wall thickness of 160 μm (Figure 2b). Further control over the number and the arrangement of channels was demonstrated by a four-channeled NF scaffold (Figure 2c) and a seven-channeled NF scaffold (Figure 2d). The four-channeled SW PLLA scaffold was presented as a control (Figure 2e). The channel walls of the NF scaffolds were composed of interconnected nanofibers. In contrast, there were no nanofibers on the walls of SW scaffolds (Figure 3).

Important structural characteristics of the NF scaffolds are listed in Table 1. The average fiber diameter of the channel wall was ≈150 nm and did not change significantly with the polymer concentration, while the porosity and average fiber length decreased with increasing polymer concentration. All the NF scaffolds had surface-area-to-volume ratios ($>70\,m^2 \cdot g^{-1}$) thousands of times higher than those of SW scaffolds ($\approx 0.027\,m^2 \cdot g^{-1}$) and did not change significantly with the change in polymer concentration.

The tensile mechanical properties of the NF scaffolds prepared from different polymer concentrations were measured along the longitudinal direction. The tensile modulus, tensile strength, and elongation at break all increased with polymer concentration (Figure 4).

The NF scaffolds adsorbed nearly 50 times more BSA than the SW scaffolds (Figure 5a). A much stronger fluorescence was emitted from the adsorbed FITC-conjugated BSA on the NF scaffolds (Figure 5b) than that on the SW scaffolds (Figure 5c).

To investigate the effect of surface morphology on cell attachment and distribution, PC12 cells and rabbit patellar tendon FBs were seeded and cultured on NF films, SW films, and single channeled NF and SW scaffolds. The cell number on NF films was significantly higher than that on SW films after 2 h of cell seeding (Figure 6). After cells were cultured within the single channeled scaffolds for 4 d, more uniform cell distribution and higher cell numbers were observed on the NF scaffolds than on the SW scaffolds (Figure 7).

4. Discussion

There are many tissues that have bundled fibrillar or tubular ECM structures.[29] For instance, the peripheral nerve sheaths are closely packed into fascicles to facilitate the prompt and accurate signal transduction.[12] Multi-channeled scaffolds that mimic the tubular bundle structure have been demonstrated to enhance axon extension as well as to guide directional re-innerva-

Table 1. Structural parameters of NF PLLA scaffolds prepared with varying polymer concentrations.

Concentration [% w/v]	Fiber diameter [nm]	Fiber length [nm]	Density $[g \cdot mL^{-1}]$	Porosity [%]	Specific surface area $[m^2 \cdot g^{-1}]$
6	157 ± 21	1250 ± 182	0.101	92.0	72.6 ± 4.0
8	155 ± 19	994 ± 107	0.123	90.2	72.7 ± 6.0
10	154 ± 30	700 ± 79	0.164	87.0	76.0 ± 5.9
12	161 ± 31	556 ± 60	0.186	85.2	72.5 ± 4.3

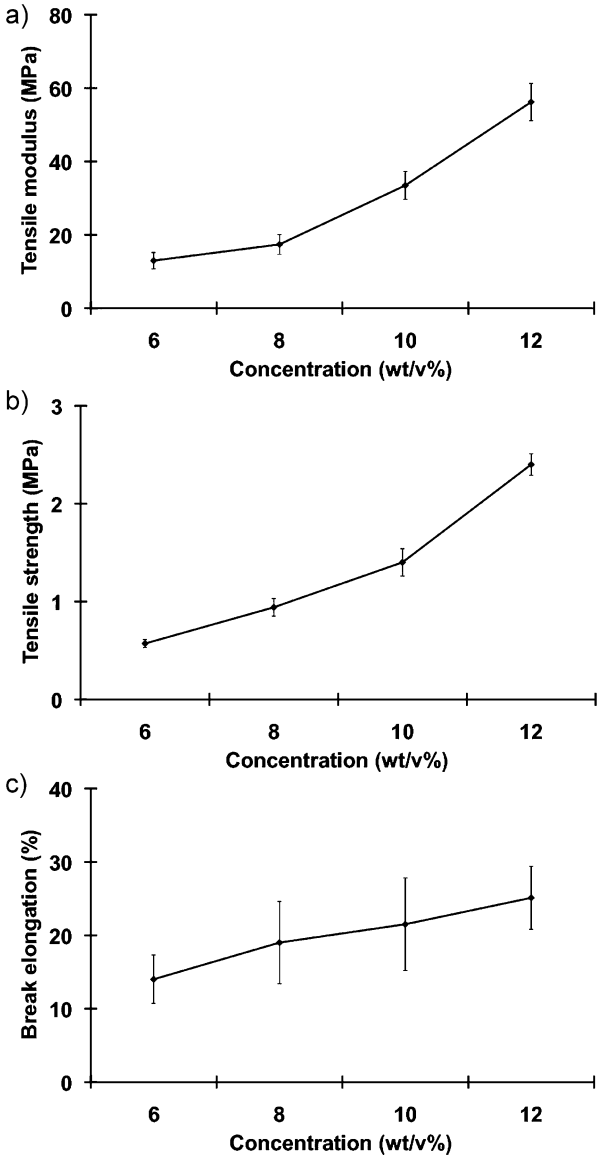

Figure 4. The effects of PLLA concentration on the mechanical properties of fabricated NF PLLA scaffolds. (a) Tensile modulus, (b) tensile strength, and (c) elongation at break.

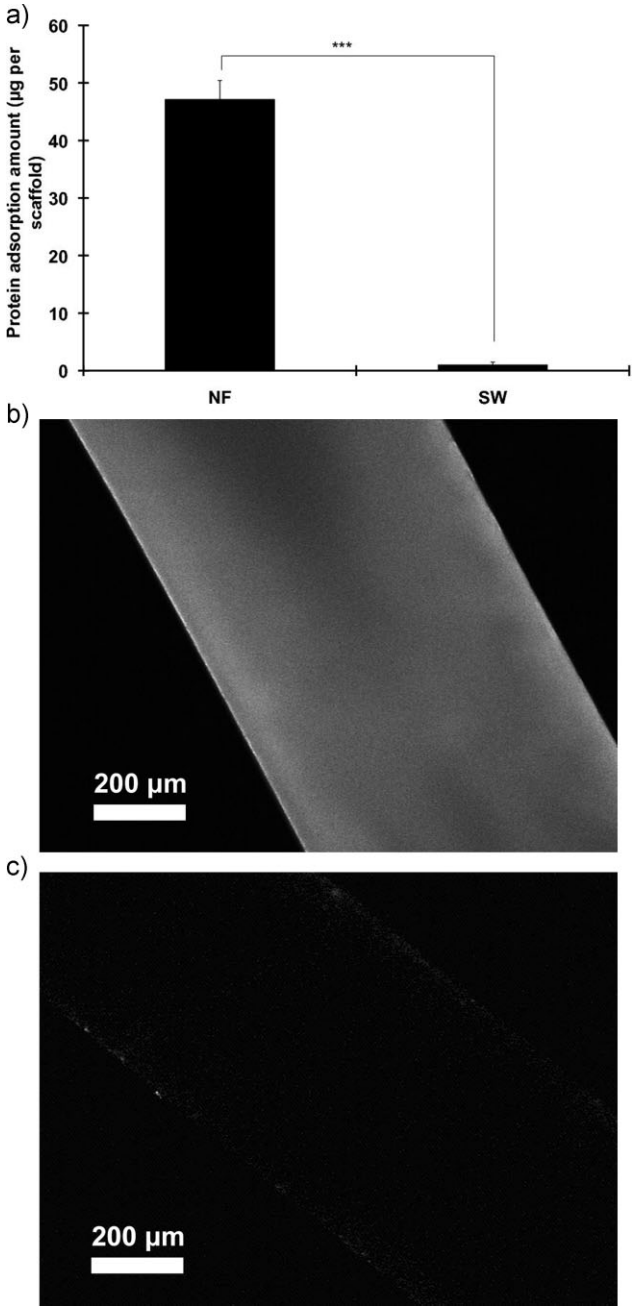

Figure 5. Protein adsorption on NF and SW PLLA scaffold: (a) much higher amount of BSA protein was adsorbed onto NF scaffolds than onto SW scaffolds after soaked in 1% BSA solution for 2 h ($^{*}p < 0.001$); (b) a fluorescent image of BSA-adsorbed NF scaffold; and (C) a fluorescent image of BSA-adsorbed SW scaffold. Much stronger fluorescence from the NF scaffold indicated much more FITC-conjugated BSA was adsorbed onto the NF scaffold than on the SW scaffold.

tion.[14,30] The channel number and dimensions were found to affect the axonal sprouting and functional recovery.[31,32] However, the existing techniques for creating a channeled structure are limited and are unable to generate channeled NF scaffolds.

In the present study, a new technique that combines injection molding and phase separation was developed to generate NF scaffolds with controllable channels. The spacers were an important aspect of the mold design. With the use of spacers, a varying number of needles were assembled into a glass tube (Figure 1). The spacers held the needles in position, allowing polymer solution to flow through the helical openings of the helical tapes and the gaps among the tubular sleeves. The spacers could be easily removed to facilitate demolding process. A channeled NF scaffold was generated after the phase separation of the polymer solution and the removal of the needles. The

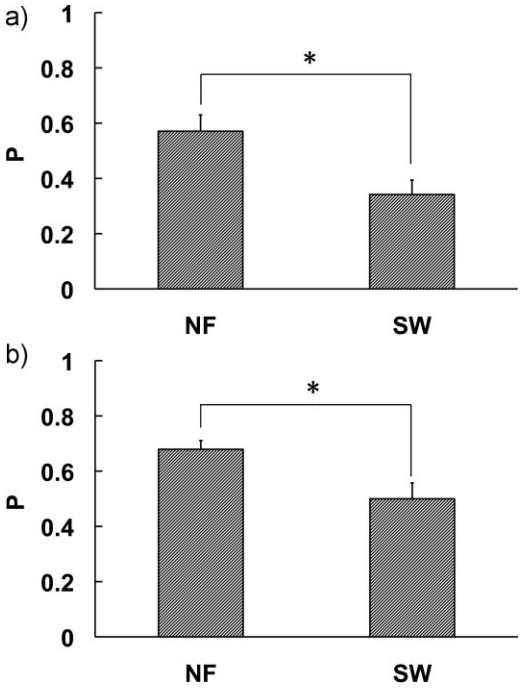

Figure 6. Proportion of cell attachment (P) on NF and SW films: (a) PC12 cells, (b) patellar tendon FB cells, $^{*}p < 0.05$.

resulting scaffold was the negative replica of the mold, where the longitudinally aligned channels were defined by the needles and the channel wall thickness was controlled by the thickness of spacers. This technique is capable of tailoring the external and internal structures of the scaffold, including the macro-scale tubular shape, the micro-scale channels, and the nano-scale fibers of the channel walls, which are intended to facilitate cell adhesion, mass transport, and oriented tissue formation.

A channeled conduit with semi-permeable wall architecture promotes nutrient exchange and prevents the infiltration of granulation cells that contribute to scarring and loss of tissue function.[33,34] Different types of porous walls were previously created using porogen leaching[35] or gas foaming[36] techniques. However, one of the limitations of these foaming techniques is the inability to create the ECM-mimicking NF structure. Another limitation is that the pores are not uniformly distributed, reducing wall integrity and mechanical properties, which in turn increase the risk of scaffold deformation and collapse.[30] In the current study, the pores are continuously distributed throughout the channel walls. The highly interconnected small pores can facilitate the diffusion of nutrients, signaling molecules, and metabolic byproducts while preventing the

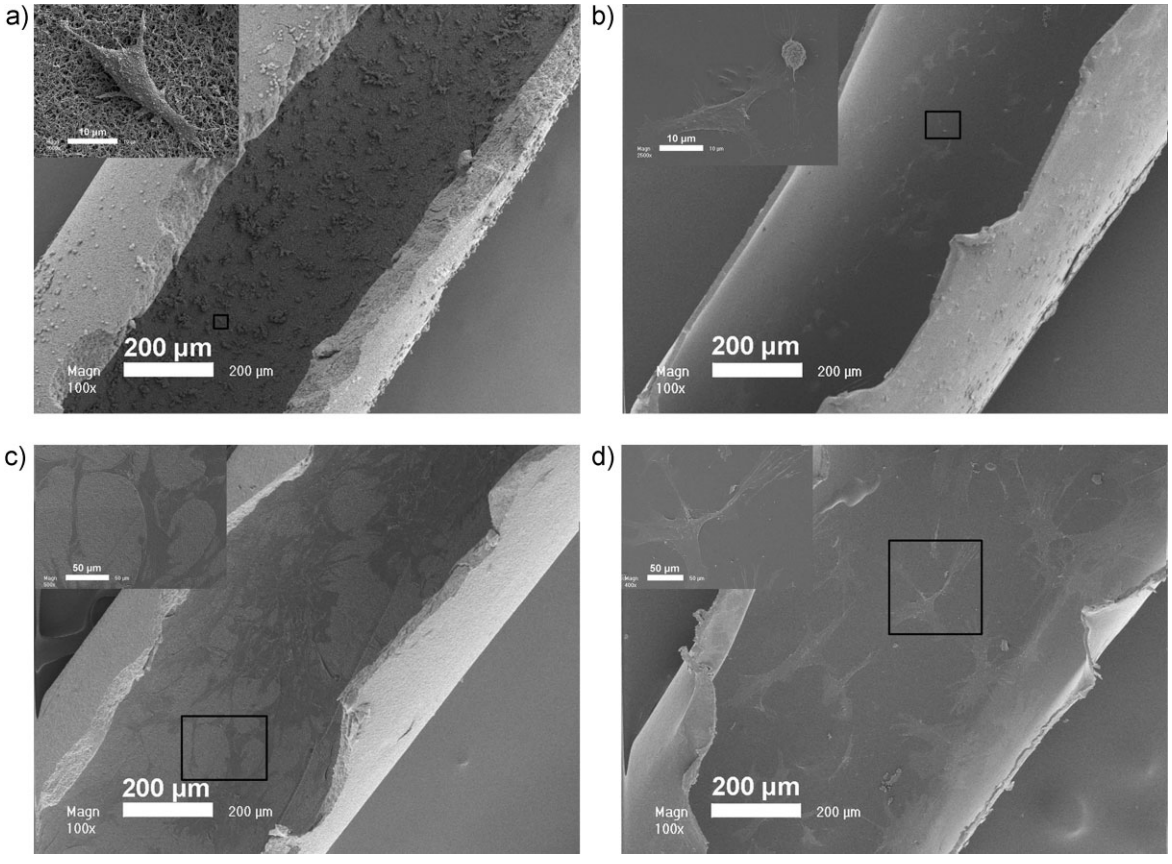

Figure 7. SEM micrographs of PC12 cells and patellar tendon FB cells cultured on NF and SW scaffolds for 4 d: (a) PC12 cells on NF scaffold; (b) PC12 cells on SW scaffold; (c) patellar tendon FB cells on NF scaffold; and (d) patellar tendon FB cells on SW scaffold.

infiltration of unwanted cells. In a previous study in our lab, it was demonstrated that NF scaffolds exhibited significantly better mechanical properties than the control SW scaffolds of similar porosities.[37,38] In this study, we demonstrated the ways to tailor the mechanical properties of the new channeled NF scaffolds, potentially matching the needs for various tissue engineering applications.

Nanofibrous (NF) scaffolds have been previously shown to enhance bone and cartilage tissue regeneration.[7,9,10,39] Cell adhesion to the scaffold is an important process in tissue engineering. Material surface modification using peptides,[40,41] proteins,[42,43] and polymers[44] have been shown to effectively enhance cell adhesion to substrates.[45] However, the effect of topographical architecture of scaffold on cell adhesion has not been well investigated. In this work, we showed that the channeled NF scaffolds had a surface area more than three orders of magnitude greater than that of the control SW scaffolds. The NF scaffolds also dramatically increased the protein adsorption capacity over the control SW scaffolds. It was also shown that significantly more neuronal PC12 cells and tendon FB cells adhered to the NF scaffolds than those adhered to the control SW scaffolds, which were likely associated with the abundantly adsorbed proteins on the NF scaffolds. Taken together, the channeled NF scaffolds are of great potential for constructing longitudinally aligned tissues. The new fabrication technique also allows for easy control over the channel size, which will be utilized to optimize cell polarization and to facilitate the orientation of regenerating tissues in future studies.

5. Conclusion

NF PLLA scaffolds with longitudinally oriented single channel or multiple channels were fabricated by combining injection molding and TIPS techniques. The scaffolds exhibited high channel wall porosities, high surface areas, and tunable mechanical properties. The porous NF channel wall matrix provides an advantageous luminal surface for cell adhesion and growth. Therefore, the anatomically shaped and ECM-mimicking channeled NF scaffolds have potentials for the engineering of longitudinally orientated bundle tissues, such as nerve and tendon.

Acknowledgements: This work was financially support by the National Institutes of Health (Research Grants DE015384 and DE017689: PXM). C. S. was a visiting student from South China University of Technology and was partially supported by the China Scholarship Council.

Received: January 5, 2012; Revised: February 19, 2012; Published online: April 16, 2012; DOI: 10.1002/mabi.201200004

Keywords: fibers; nerves; scaffolds; tendons; tissue engineering

[1] R. Langer, J. Vacanti, *Science* **1993**, *260*, 920.
[2] P. X. Ma, *Adv. Drug Delivery Rev.* **2008**, *60*, 184.
[3] A. Khademhosseini, R. Langer, J. Borenstein, J. P. Vacanti, *Proc. Natl. Acad. Sci. USA* **2006**, *103*, 2480.
[4] N. C. Rivron, J. Rouwkema, R. Truckenmuller, M. Karperien, J. De Boer, C. A. Van Blitterswijk, *Biomaterials* **2009**, *30*, 4851.
[5] P. Benya, J. Shaffer, *Cell* **1982**, *30*, 215.
[6] C. L. Murphy, A. Sambanis, *Tissue Eng.* **2001**, *7*, 791.
[7] K. M. Woo, J.-H. Jun, V. J. Chen, J. Seo, J.-H. Baek, H.-M. Ryoo, G.-S. Kim, M. J. Somerman, P. X. Ma, *Biomaterials* **2007**, *28*, 335.
[8] W. J. Li, R. Tuli, X. Huang, P. Laquerriere, R. S. Tuan, *Biomaterials* **2005**, *26*, 5158.
[9] J. Hu, K. Feng, X. H. Liu, P. X. Ma, *Biomaterials* **2009**, *30*, 5061.
[10] X. Liu, X. Jin, P. X. Ma, *Nat. Mater.* **2011**, *10*, 398.
[11] N. L. Nerurkar, B. M. Baker, S. Sen, E. E. Wible, D. M. Elliott, R. L. Mauck, *Nat. Mater.* **2009**, *8*, 986.
[12] C. E. Schmidt, J. B. Leach, *Ann. Rev. Biomed. Eng.* **2003**, *5*, 293.
[13] Y. Liu, H. S. Ramanath, D.-A. Wang, *Trends Biotechnology* **2008**, *26*, 201.
[14] M. J. Moore, J. A. Friedman, E. B. Lewellyn, S. M. Mantila, A. J. Krych, S. Ameenuddin, A. M. Knight, L. Lu, B. L. Currier, R. J. Spinner, R. W. Marsh, A. J. Windebank, M. J. Yaszemski, *Biomaterials* **2006**, *27*, 419.
[15] J. Y. Lee, C. A. Bashur, N. Gomez, A. S. Goldstein, C. E. Schmidt, *J. Biomed. Mater. Res., A* **2010**, *92*, 1398.
[16] R. James, S. G. Kumbar, C. T. Laurencin, G. Balian, A. B. Chhabra, *Biomed. Mater.* **2011**, *6*, 025011.
[17] C. Sundback, T. Hadlock, M. Cheney, J. Vacanti, *Biomaterials* **2003**, *24*, 819.
[18] T. Hadlock, J. Elisseeff, R. Langer, J. Vacanti, M. Cheney, *Arch. Otolaryngol. Head Neck Surg.* **1998**, *124*, 1081.
[19] L. Flynn, P. D. Dalton, M. S. Shoichet, *Biomaterials* **2003**, *24*, 4265.
[20] S. Stokols, J. Sakamoto, C. Breckon, T. Holt, J. Weiss, M. H. Tuszynski, *Tissue Eng.* **2006**, *12*, 2777.
[21] R. G. Flemming, C. J. Murphy, G. A. Abrams, S. L. Goodman, P. F. Nealey, *Biomaterials* **1999**, *20*, 573.
[22] Z. M. Huang, Y. Z. Zhang, M. Kotaki, S. Ramakrishna, *Compos. Sci. Technol.* **2003**, *63*, 2223.
[23] L. A. Smith, X. H. Liu, P. X. Ma, *Soft Matter* **2008**, *4*, 2144.
[24] F. Gelain, A. Horii, S. G. Zhang, *Macromol. Biosci.* **2007**, *7*, 544.
[25] P. X. Ma, R. Y. Zhang, *J. Biomed. Mater. Res.* **1999**, *46*, 60.
[26] X. Liu, P. X. Ma, *Biomaterials* **2009**, *30*, 4094.
[27] L. A. Smith, X. H. Liu, J. A. Hu, P. X. Ma, *Biomaterials* **2010**, *31*, 5526.
[28] K. M. Woo, V. J. Chen, P. X. Ma, *J. Biomed. Mater. Res., Part A* **2003**, *67A*, 531.
[29] P. X. Ma, R. Y. Zhang, *J. Biomed. Mater. Res.* **2001**, *56*, 469.
[30] G. C. de Ruiter, R. J. Spinner, M. J. A. Malessy, M. J. Moore, E. J. Sorenson, B. L. Currier, M. J. Yaszemski, A. J. Windebank, *Neurosurgery* **2008**, *63*, 144.
[31] L. Yao, G. C. W. de Ruiter, H. Wang, A. M. Knight, R. J. Spinner, M. J. Yaszemski, A. J. Windebank, A. Pandit, *Biomaterials* **2010**, *31*, 5789.
[32] A. J. Krych, G. E. Rooney, B. Chen, T. C. Schermerhorn, S. Ameenuddin, L. Gross, M. J. Moore, B. L. Currier, R. J. Spinner,

J. A. Friedman, M. J. Yaszemski, A. J. Windebank, *Acta Biomater.* **2009**, *5*, 2551.
[33] C. B. Jenq, R. E. Coggeshall, *Brain Res.* **1985**, *361*, 233.
[34] C. L. A. M. Vleggeert-Lankamp, G. C. W. de Ruiter, J. F. C. Wolfs, A. P. Pego, R. J. van den Berg, H. K. P. Feirabend, M. J. A. Malessy, E. A. J. F. Lakke, *J. Biomed. Mater. Res., Part A* **2007**, *80A*, 965.
[35] L. He, Y. Zhang, C. Zeng, M. Ngiam, S. Liao, D. Quan, Y. Zeng, J. Lu, S. Ramakrishna, *Tissue Eng. C* **2009**, *15*, 243.
[36] Y. Yang, L. De Laporte, C. B. Rives, J. H. Jang, W. C. Lin, K. R. Shull, L. D. Shea, *J. Controlled Release* **2005**, *104*, 433.
[37] P. X. Ma, J. W. Choi, *Tissue Eng.* **2001**, *7*, 23.
[38] V. J. Chen, P. X. Ma, *Biomaterials* **2004**, *25*, 2065.
[39] V. J. Chen, L. A. Smith, P. X. Ma, *Biomaterials* **2006**, *27*, 3973.
[40] M. H. Ho, L. T. Hou, C. Y. Tu, H. J. Hsieh, J. Y. Lai, W. J. Chen, D. M. Wang, *Macromol. Biosci.* **2006**, *6*, 90.
[41] J. F. Alvarez-Barreto, V. I. Sikavitsas, *Macromol. Biosci.* **2007**, *7*, 579.
[42] K. Vallieres, E. Petitclerc, G. Laroche, *Macromol. Biosci.* **2007**, *7*, 738.
[43] W. B. Tsai, M. C. Wang, *Macromol. Biosci.* **2005**, *5*, 214.
[44] B. Cao, S. F. Yan, K. X. Zhang, Z. J. Song, T. Cao, X. S. Chen, L. Cui, J. B. Yin, *Macromol. Biosci.* **2011**, *11*, 970.
[45] X. Liu, J. M. Holzwarth, P. X. Ma, *Macromol. Biosci.* **2012**, in press, DOI: 10.1002/mabi.201100466.